Journal of Geoscience and Environment Protection, 2022, 10, 204-224
https://www.scirp.org/journal/gep
ISSN Online: 2327-4344
ISSN Print: 2327-4336

Determination of the Aquifer and Its Hydraulic Parameters Using Vertical Electrical Sounding, Borehole Log Data and Borehole Water Conductivity: A Case Study of Olbanita Menengai Area, Nakuru, Kenya

Daniel Mogaka Nyaberi

Department of environmental Earth Sciences, University of Eldoret, Uasin Gishu, Kenya
Email: nyaberimogaka@gmail.com

How to cite this paper: Nyaberi, D. M. (2022). Determination of the Aquifer and Its Hydraulic Parameters Using Vertical Electrical Sounding, Borehole Log Data and Borehole Water Conductivity: A Case Study of Olbanita Menengai Area, Nakuru, Kenya. *Journal of Geoscience and Environment Protection, 10,* 204-224.
https://doi.org/10.4236/gep.2022.1011014

Received: November 3, 2022
Accepted: November 25, 2022
Published: November 28, 2022

Abstract

Development of groundwater needs the capabilities to distinguish the different aquifer layers found in a region, and thereafter the parameters which can be used expressly to define the aquifer type. The past studies in the Olbanita sub-basin have accorded the area as having one aquifer, which has resulted into generalization of the aquifer parameters. The objective in this study is to map the main aquifer layer and determine its parameters. The use of modeled geoelectric layers from Vertical Electrical Sounding (VES) data has been used in the study area to distinguish the major aquifer from the minor ones. There is noted an excellent correlation between the geoelectric layers and the lithologies as outlined by the driller's log clearly delineating four aquifer stratums. The main aquifer is identified to be geoelectric layer 11 and 12, defined by a thickness of 30.18 m mainly of tuffs, and 17.39 m mainly of weathered phonolites. Hydraulic conductivity of the main aquifer averages value of 17.16389314 m/day, in consideration of the ranges 0.248690465 m/day to 74.62681942 m/day for the 31 VES points. For the aquifer breadth of 30.18 m, the Transmissivity values vary from a minimum of 57.32119 Ωm^2 to 53365.49 Ωm^2 and for 47.57 m breadth, the range is between 11.83021 Ωm^2 and 1390.921 Ωm^2. The variance of longitudinal unit conductance shows that 63.15 percent of the aquifer represented by one lithology is having lowest values of S (<1.0 Ω^{-1}), an indication that the resistivity values of these points are relatively high when compared to their corresponding breadths. Notably, where the geoelectric layer is represented by more than one lithologic layer, the longitudinal unit conductance has high values of S (~1.1 - 5.3 Ω^{-1}) at about 83.33 percent

of the aquifer, thus giving a manifestation that a change in lithology has an implication in the aquifer characteristics. The transverse resistance values have a direct proportionality to both the aquifer layer thickness and the geoelectric layer resistivities. Evidently, using the close range of resistivities record indicates that indeed transverse resistance increases with increase in aquifer thickness. For example, for resistivities 52.677 Ω, 54.78 Ω, 54.297 Ω, 57.819 Ω, and 51.85 Ω, for 30.18 m, 47.57 m, 136.35 m, 190.84 m, 277.93 m thicknesses respectively, have their correlated transverse resistances values notably rising incrementally, from 1589.7919 Ωm^2, 2605.8846 Ωm^2, 7403.396 Ωm^2, and 11034.178 Ωm^2 correspondingly. There is confirmation that the modeled VES data can help map aquifers despite the limited resources of borehole logs that can used as control points.

Keywords

Aquifer, Hydraulic Conductivity, Transmissivity, Longitudinal Unit Conductance, Transverse Resistance

1. Introduction

Freshwater is a finite and vulnerable resource with many people still lacking access to adequate supply for basic needs hampered by the global increase in economic activities and improved standards of living leading to amplified competition for, and conflicts over the limited freshwater resource (Nyaberi, 2010). Despite the global challenges, still groundwater offers indispensable potential of enhancing water provisions, especially in supporting the rural communities (Nyaberi, 2020). According to Nyaberi (2010), groundwater from Kabatini, Baharini, Olobanita well fields forms a major source of fresh water supply to Nakuru City.

Several studies have been carried out in the Olbanita sub-basin, overarching groundwater quality, subsurface structure, subsurface temperatures, groundwater development, and groundwater evolutionary processes. It is evident that the past researches treats the groundwater regime in the area as just one aquifer layer, or otherwise as one that can be defined using average parameters despite the different lithologies. A study carried out by Sosi (2020), assumably considers the aquifer as one unit where anomalies in aquifer transmissivity and hydraulic conductivity are only noted in the N-S fault-fractures and not noted to be related to the aquifer lithologies. The application of boreholes' data has been used to establish the existence of two highly conductive coarse sand aquifer layers in the Olobanita area with high yields of 40 to over 60 m^3/h occurring at depths of 104 - 118 m and 119 - 128 m (Olago, 2018) without much correlation to other aquifer lithologic materials. The noticeable acknowledgement of existence of best aquifers made of weathered tuffs sandwiched between the Samburu basalts and the Wasagess flows by Sosi et al. (2019), qualifies that there are more than one layer of aquifer but not clearly enumerated. This study seeks to distinguish the

main aquifer from the rest and its related aquifer parameters.

Geophysical techniques are gradually being deployed for subsurface characterization, and so is the application to groundwater studies. Traditionally, pumping tests have been used for the estimation of the hydraulic parameters of the aquifer, an aspect which has limited studying aquifers given the resources needed to drill boreholes before getting pumping tests' data. A geophysical survey is often the most cost-effective and rapid means of obtaining subsurface information, especially over large study areas (Sirles, 2006). Using geophysical tools during the initial characterization is an intuitive process offering rapid insight into subsurface physical properties. Notably, the electrical resistivity method is one of the most useful techniques in groundwater hydrology exploration, because the resistivity of a rock is very sensitive to its water content. In turn, the resistivity of water is very sensitive to its ionic content. It is cheap to deploy vertical electrical sounding (VES) to collect data from a large area and use the same in estimation of the hydraulic parameters of an aquifer. In this study, an attempt is made to map the main aquifer in Olbanita sub-basin and estimate its hydraulic parameters using the VES data. Thus, the research applies the analysis of the Vertical Electrical Resistivity Sounding data in the estimation of hydraulic parameters' of the aquifer in the study area.

2. Materials and Methods

2.1. Study Area

The study area is a volcano-sedimentary sub-basin, part of Olobanita well-field found in Menengai, sheet 119/1, and is located within the Lower Baringo Basin, Central Kenya Rift. In a magnified scale, the area can be defined by UTM coordinates of 37 M 0178000, UTM 998400; 37 M 0179200, UTM 998400; 37 M 0179200, UTM 998600; and 37 M 0178000, UTM 998600, as shown in **Figure 1**. The Olobanita well-field is bounded by Bahati hills to the East, Menengai caldera to the South, Solai escarpment to the North and El Bonwala Hill to the North West. The study area is part of the 7.5 kilometers square region where groundwater exploitation boreholes are drilled to supply water to Nakuru City.

Kenyan Rift Valley's geology at large and for Olbanita area in specific is characterized by rocks representing lava flows, superficial sediments, and soils (Olago, 2018) whose origin is associated to magma deposition from fissuring and faulting within the rift valley (McCall, 1967). Structurally, the area is characterized by E-W extension tectonics where tensional forces resulted in block faulting. This included tilted blocks as evident in both the floor and scarps of the rift. Evidence obtained based on geologic logs from borehole data used by Nyaberi (2010) in his research indicates that the area is characterized by periodic sequences of volcanic activity. This is supported by Olago (2018) whose work has defined the occurrence of the volcanic activity to be of the Late Pleistocene that constitutes phonolytic trachytes and sometimes the welded vitreous tuffs and ignimbrites.

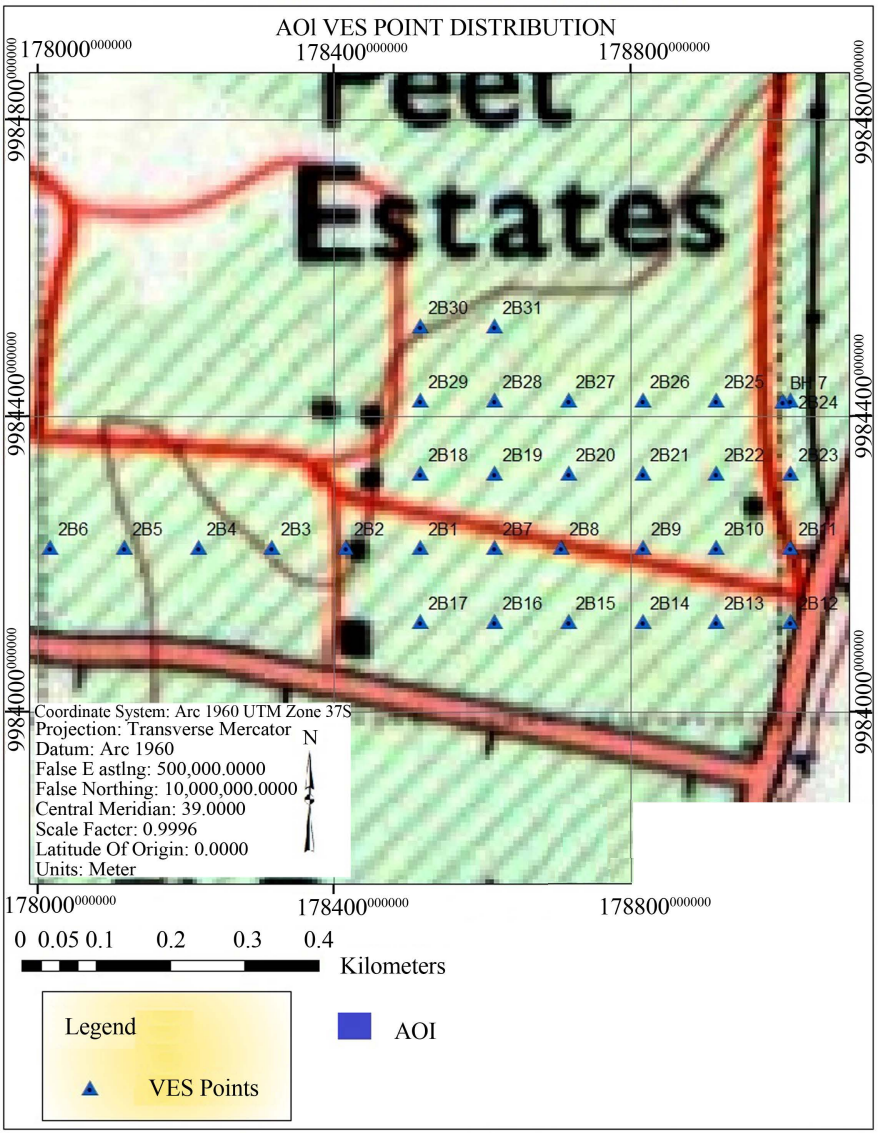

Figure 1. Location of the study area showing points where VES data were collected.

2.2. Vertical Electrical Sounding Method

The data collection by VES method was realized by deploying the Schlumberger array with the use of the Abem SAS 1000 Terrameter resistivity meter. In the Schlumberger array four electrodes; A and B (current electrodes), and M and N (potential electrodes) are used in probing the subsurface (**Figure 2**) and 31 data sets were collected with VES 24 carried out on the same spot with BH 7, as publicised in **Figure 1**.

The software (EarthImager 1D) used in VES data analysis considers application of data in the form *V*/*I*, while the field data is collected in the format of resistivity, thus conversion of data sets is necessary. The relationship between *V*/*I* and resistivity is given as shown in Equation (1).

$$\rho = 2\pi \frac{\Delta v}{I} k \tag{1}$$

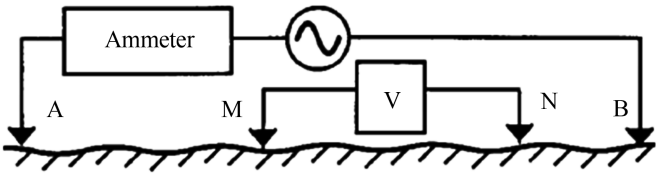

Figure 2. General configuration of the four surface electrodes in linear resistivity surveys with current delivered through the electrodes A and B, and voltage readings are made through M and N. (after Rhett H. 2001).

where ΔV is the voltage drop or potential difference from one end of a resistor to another, ρ is the resistivity, K is the geometric factor and 2π is derived from the halfspace of area $\frac{1}{2}\left(4\pi r^2\right)$ of the spherical earth, due to a point current source of strength I in an infinite medium gives (Equation (2)):

$$V = \frac{\rho I}{2\pi r} \tag{2}$$

The field data collection is carried out on the surface of the earth, which is a sphere in nature with the point current source where a known current is put into the ground and measurement of the resulting voltage drop used to estimate the resistivity of the subsurface. Depending on the focus potential electrode, the voltage can be treated as v_M or v_N and thus the total current (I) flows away from or toward the electrode across the surface of a half sphere and with the distances between the electrodes given by r_{11}, r_{12}, etc., and $V = 0$ infinitely far from the current source, the potentials at M and N are given by (Rhett, 2001) as Equations (3) and (4):

$$v_M = \frac{\rho I}{2\pi}\left[\frac{1}{r_{11}} - \frac{1}{r_{21}}\right] \tag{3}$$

$$v_N = \frac{\rho I}{2\pi}\left[\frac{1}{r_{12}} - \frac{1}{r_{22}}\right] \tag{4}$$

and the combination of the two Equations (3) and (4) gives a complete resultant in field measurement where the outcome equation is given as (Equation (5)):

$$\Delta v = v_1 - v_2 = \frac{\rho I}{2\pi}\left[\frac{1}{r_{11}} + \frac{1}{r_{22}} - \frac{1}{r_{21}} - \frac{1}{r_{12}}\right] \tag{5}$$

where the K applied to the Schlumberger configuration is given from the relationship (Equation (6)) and is determined by the relationship between AB and MN distances in the field measurements:

$$\frac{1}{k} = \frac{1}{r_{11}} + \frac{1}{r_{22}} - \frac{1}{r_{21}} - \frac{1}{r_{12}} \tag{6}$$

Otherwise, given the heterogeneity of geology, the resistivity is presented as apparent resistivity, and in cases where r_{11}, r_{12}, r_{21}, r_{22} values are given in metres, and Δv and I in measured in millivolts and milli amperes respectively, then the pa would be in ohm-meters.

2.3. Data Processing and Analysis

The VES data was collected where the Schlumberger array was deployed at thirty one locations (31) in the study area where apparent resistivity values were collected using the ABEM SAS 1000 Terrameter. In the field, a 12 V DC power source was used in powering the Terrameter. The four electrodes were inserted into the ground following the Schlumberger configuration, and subsequently raw resistivity data collected.

The data processing criteria was based on the Schlumberger array used and the subsequent data collected. This formed the first phase of processing among two used in data processing. This first phase was digitally achieved with ABEM SAS 1000 Terrameter data handling internal capabilities where the instructions keyed into the equipment when collecting the data formed the basis. The current was imparted into the ground using two electrodes (C+ and C−) defining AB (happening in an alternating manner), and the voltage drop is measured between the two other electrodes (P1 and P2) defining MN as shown in **Figure 2**, and the continuous adjustment on the ground as necessary as the key inputs into the procedure thus forming the protocol used in data processing.

3. Estimation of Hydraulic Parameters

The formation water resistivity, σ, is defined as the reciprocal of water conductivity (Equation (7)). The overall rock resistivity to the respectabilities of a clay-free (clean), saturated aquifer is given through Archie's Law as given in Equation (8) (Archie, 1942, 1950):

$$\rho = \frac{1}{\sigma} \tag{7}$$

$$\rho_r = a\rho_w \varphi^{-m} \tag{8}$$

where, *a*, *is* the tortuosity (lithology factor), *m* is cementation exponent and φ is porosity where the $m = 2.0$ for rock with small fissures and $m = 1.64$ - 2.23 for Natural sediment (Byun et al., 2019). The negative correlation in power *m* indicates that the porosity increases with a decrease in total porosity. Tortuosity factor is a significant parameter in formation resistivity factor calculations in the Archie formula, which is used to predict water saturation, taken as a unity, $a \approx 1$ for fully saturated rocks (Byun et al., 2019). This generalization of tortuosity factor, a, was destined so as the Archie relationship could accommodate a variety of sandstone types (Winsauer et al., 1952). Notably, in most cases the Archie's parameters *a*, *m* are usually held constant thus, the change in lithology with depth in a heterogeneous reservoir is ignored, even with the knowledge that these parameters have the largest influence in calculation of water saturation (Hamada et al., 2012; Pinas & Elias, 2019). Accordingly, different *a*, and *m* values have been documented for different types of formations (**Table 1**).

In this study $a = 1$, $m = 2.0$ are used with the consideration that the resultant geology is from deposition of fine material from volcanic ashes as noted by

Table 1. Different *a* and *m* values have been documented for different types of formations (Pinas & Elias, 2019).

a: Tortuosity factor	*m*: Cementation exponent	Comments
1.0	2.0	Carbonates*
0.81	2.0	Consolidated sandstones*
0.62	2.15	Unconsolidated sands (Humble Formula)*
1.45	1.54	Average sands (Carothers, 1968)
1.65	1.33	Shaly sands (Carothers, 1968)
1.45	1.70	Calcareous sands (Carothers, 1968)
0.85	2.14	Carbonates (Carothers , 1968)
2.45	1.08	Pliocene sands,, southern California (Carothers & Porter, 1970)
1.97	1.29	Miocene sands, Texas-Louisiana Gulf Coast (Carothers & Porter, 1970)
1.0	$\varnothing^{(2.05-\varnothing)}$	Clean granular formations (Sethi, 1979)

*Most commonly used.

Nyaberi (2010). The formation resistivity factor, *F*, is defined as the ratio of the rock resistivity fully saturated with water content (R_o) to the ratio of the resistivity of water contained, R_w, (Equation (9)).

$$F = \frac{\rho_r}{\rho_w} \tag{9}$$

According to Salem (2001), the hydraulic conductivity *K* can be calculated as shown in Equation (10). Thus, the intrinsic permeability and hydraulic conductivity can be related using Equation (11) after Nutting (1930);

$$K = 7.7 \times 10^{-6} F^{2.09} \tag{10}$$

$$K = \left(\frac{\delta_w g}{\mu}\right) k_f \tag{11}$$

where δ_w is the fluid density (1000 kg/m^3), μ is the dynamic viscosity of water (0.0014 kg/ms), *g* is acceleration due to gravity (9.81 m/s^2). Using the Kozeny-Carmen-Bear equation (Carmen, 1956; Kozeny, 1953), the hydraulic conductivity K can be calculated as shown in Equation (12):

$$K = \left(\frac{\delta_w g}{\mu}\right)\left(\frac{d^2}{180}\right)\left[\frac{\varphi^3}{(1-\varphi)^2}\right] \tag{12}$$

where *d* is the grain size and unit of *K* being m/sec. Accordingly, using the rela-

tionship between the hydraulic conductivity K and the thickness b the transmissivity (T) of the aquifer is as shown in Equation (13):

$$T = Kb \tag{13}$$

and the Equations (14) and (15) gives the relationship between the hydraulic conductivity K, electrical resistivity ρ of an aquifer, and the transmissivity of the aquifer;

$$T = (k\rho)S \tag{14}$$

and

$$S = \frac{h}{\rho} \tag{15}$$

where ρ is the bulk resistivity, S is the longitudinal unit conductance and h is the aquifer thickness. For a lateral hydraulic flow and current flowing transversely, the transmissivity of the aquifer becomes Equations (16) and (17);

$$T = \frac{K}{\rho}R \tag{16}$$

and

$$R = h\rho \tag{17}$$

where R is the transverse unit resistance of the aquifer. If the aquifer is saturated with water with uniform resistivity, then the product $K\rho$ or K/ρ would remain constant. The above equations may therefore be written as $T = \alpha S$; $\alpha = K\rho$ and $T = \beta R$, $\beta = K/\rho$ where α and β are constants of proportionality.

4. Results

4.1. Resistivity Data Analysis

The VES data analysis was carried out for thirty one (31) points and the resultant geoelectric parameters are outlined in Table 3 and **Appendix** Table A1, where correlation of the layer models obtained from the apparent resistivity have been achieved. The VES profiles didn't manage reaching the basal layer which defines the separation between the basement system (oldest rocks) and the volcanic rocks. The resistivity-thickness reduced model is composed of sixteen layers, which in standard gives a good comparison with the lithologic layers of the borehole Olobanita BH7 driller's log (Table 2 and Table 3).

There is a considerable range of resistivities per defined layer across the VES points showing a horizontal variation, a case credited to some degree of heterogeneity, both in grain and pore characteristics and expected changing chemical characteristics of water, a situation that highly influences conductivity. The log data obtained from borehole Olobanita BH 7 drilled in the study area helped in ascertaining the resistivity variations with depth with respect to the reduced model correlated with lithology (Table 2; Figure 3). The first geoelectric layer exhibits a resistivity range of 55.01 - 158.474 Ωm, corresponding to a thickness of 8.62 m (Table A1), which represents the Top volcanic soil (Table 2 and

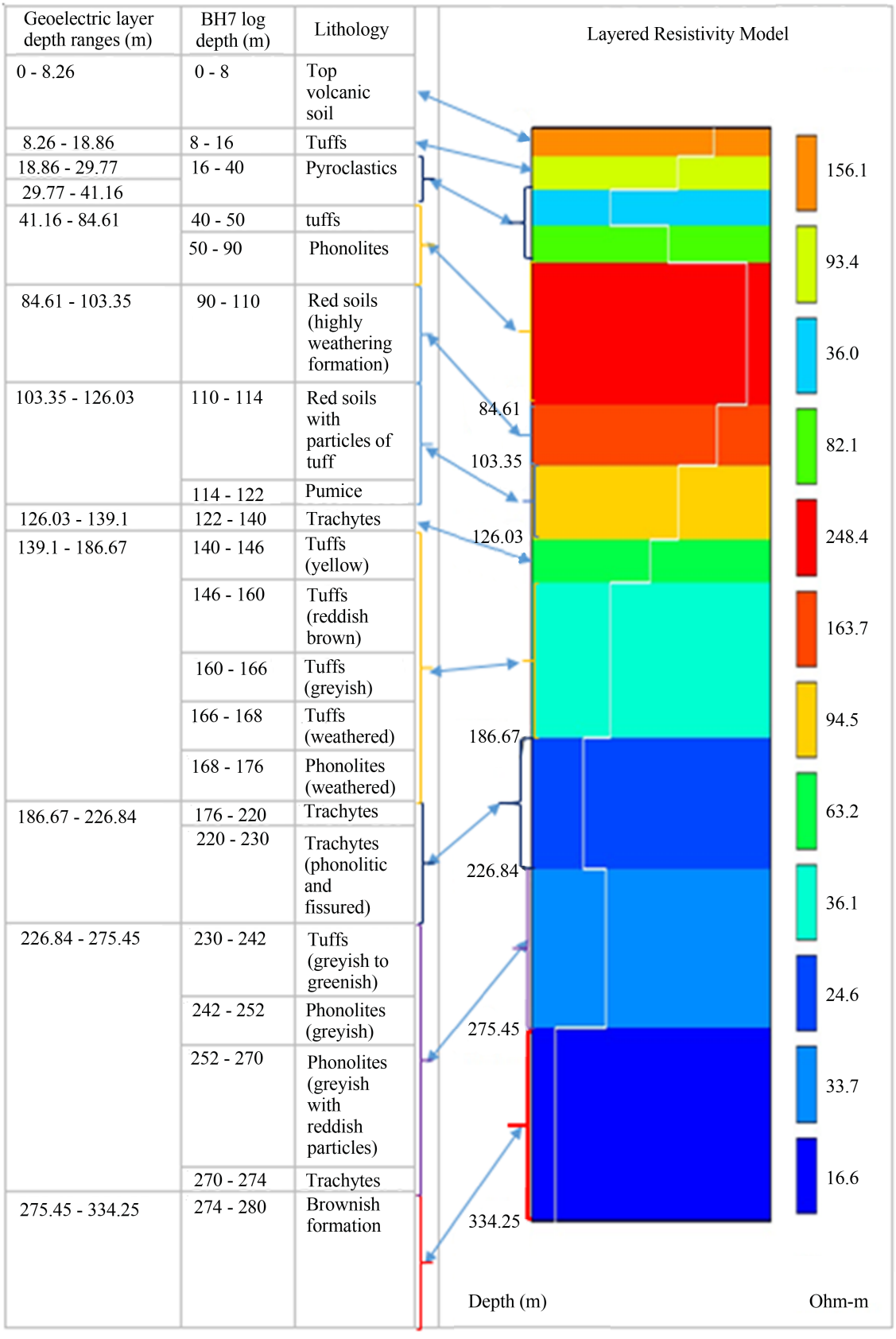

Figure 3. Comparison between lithologic log of the borehole BH7 with interpreted geoelectric layer parameters of VES point 24.

Table 2. Comparison between interpreted geoelectric layer parameters with lithological log of the borehole BH7.

Layer	Geoelectric layer depth ranges (m)	Lithologic layer depth ranges (m)	Lithology	Modeled Resistivity (Ωm)	
1	0 - 8.62	0 - 8	Top volcanic soil	156.089	Unsaturated zone
2	8.62 - 18.86	8 - 16	Tuffs	93.402	
3	18.86 - 29.77	16 - 40	Pyroclastics	35.952	
4	29.77 - 41.16			82.123	
5	41.16 - 56.32	40 - 50	tuffs	111.12	
6	56.32 - 69.12	50 - 90	Phonolites	138.256	
7	69.12 - 84.61			248.41	
8	84.61 - 103.35	90 - 110	Red soils (highly weathering formation)	163.673	
9	103.35 - 126.03	110 - 114	Red soils with particles of tuff	94.541	
		114 - 122	Pumice		
10	126.03 - 139.1	122 - 140	Trachytes	63.189	Capillary fringe
11	139.1 - 169.28	140 - 146	Tuffs (yellow)	36.098	Main aquifer
		146 - 160	Tuffs (reddish brown)		
		160 - 166	Tuffs (greyish)		
		166 - 168	Tuffs (weathered)		
12	169.28 - 186.67	168 - 176	Phonolites (weathered)	31.761	
13	186.67 - 226.84	176 - 220	Trachytes	24.561	2nd Aquifer
		220 - 230	Trachytes (phonolitic and fissured)		
14	226.84 - 249.99	230 - 242	Tuffs (greyish to greenish)	33.721	3rd aquifer
		242 - 252	Phonolites (greyish)		
15	249.99 - 275.45	252 - 270	Phonolites (greyish with reddish particles)	40.526	4th aquifer
		270 - 274	Trachytes		
16	275.45 - 334.25	274 - 280	Brownish formation	16.572	

Table 3. Sampled VES correlation of the layer models obtained from the apparent resistivity.

	1			2			3			4			5			6			7			8			9			10			11			12			13			14			15			16			
Geoelectric Layer	Starting Depth (m)	Breadth (m)	Resistivity (Ωm)	Starting Depth (m)	Breadth (m)	Resistivity (Ωm)	Starting Depth (m)	Breadth (m)	Resistivity (Ωm)	Starting Depth (m)	Breadth (m)	Resistivity (Ωm)	Starting Depth (m)	Breadth (m)	Resistivity (Ωm)	Starting Depth (m)	Breadth (m)	Resistivity (Ωm)	Starting Depth (m)	Breadth (m)	Resistivity (Ωm)	Starting Depth (m)	Breadth (m)	Resistivity (Ωm)	Starting Depth (m)	Breadth (m)	Resistivity (Ωm)	Starting Depth (m)	Breadth (m)	Resistivity (Ωm)	Starting Depth (m)	Breadth (m)	Resistivity (Ωm)	Starting Depth (m)	Breadth (m)	Resistivity (Ωm)	Starting Depth (m)	Breadth (m)	Resistivity (Ωm)	Starting Depth (m)	Breadth (m)	Resistivity (Ωm)	Starting Depth (m)	Breadth (m)	Resistivity (Ωm)	Starting Depth (m)	Breadth (m)	Resistivity (Ωm)	Starting Depth (m)
VES 10	0	8.62	131.754	8.62	21.15 m breadth 56.234 Ωm					29.77	26.55 m breadth 54.415 Ωm					56.32	12.8	82.677	69.12	15.49	152.642	84.61	18.74	311.47	103.35	22.68	527.35	126.03	13.07	337.247	139.1	30.18	587.264	169.28	17.39	330.291	186.67	40.17	400.583	226.84	107.41 m breadth 198.838 Ωm								334.25

Continued

VES 13	0	8.62	158.474	8.62	10.24	21.06	18.86	10.91	143.536	29.77	26.55 m breadth 15.482 Ωm	56.32	12.8	31.534	69.12	15.49	63.872	84.61	18.74	138.912	103.35	35.75 m breadth 344.885 Ωm	139.1	30.18	551.002	169.28	17.39	386.874	186.67	40.17	645.675	226.84	48.61 m breadth 315.04 Ωm	275.45	58.8	1059.309	334.25
VES 18	0	8.62	82.021	8.62	10.24	56.208	18.86	10.91	129.851	29.77	26.55 m breadth 374.697 Ωm	56.32	12.8	207.108	69.12	15.49	107.313	84.61	18.74	51.602	103.35	35.75 m breadth 32.539 Ωm	139.1	30.18	28.268	169.28	57.56 m breadth 47.593 Ωm	226.84	107.41 m breadth 127.829 Ωm	334.25						
VES 20	0	8.62	143.34	8.62	10.24	36.801	18.86	10.91	405.844	29.77	26.55 m breadth 112.332 Ωm	56.32	47.03 m breadth 251.418 Ωm	103.35	22.68	162.151	126.03	13.07	102.525	139.1	30.18	52.677	169.28	17.39	31.761	186.67	88.78 m breadth 11.105 Ωm	275.45	58.8	1.668	334.25					
VES 23	0	8.62	132.11	8.62	10.24	76.023	18.86	10.91	40.285	29.77	39.35 m breadth 111.12 Ωm	69.12	34.23 m breadth 167.129 Ωm	103.35	35.75 m breadth 138.915 Ωm	139.1	47.57 m breadth 82.491 Ωm	186.67	88.78 m breadth 44.74 Ωm	275.45	58.8	15.945	334.25													
VES 24	0	8.62	[illegible]	8.62	10.24	93.402	18.86	10.91	35.952	29.77	11.39	82.123	41.16	43.45 m breadth 248.41 Ωm	84.61	18.74	[illegible]	103.35	22.68	94.541	126.03	13.07	63.189	139.1	47.57 m breadth 36.098 Ωm	186.67	40.17	24.561	226.84	48.61 m breadth 33.721 Ωm	275.45	58.8	16.572	334.25		

Figure 3). The second geoelectric layer which represents the tuffs has a thickness of 10.24 m and resistivity values ranging 19.953 - 102.738 Ωm with three (3) outliers of high resistivity values.

The geoelectric layer three has a thickness of 10.91 m for 28 points, having resistivity values 129.851 - 1047.042 Ωm with seven (7) aberrations having lower resistivities. Given the good agreement between the depths given by modeled resistivity and the driller's log, then it is concluded that the resistivities of this geoelectric layer defines the same lithology. While the first two layers seemingly have considerable relatively low resistivity values, the third layer portrays relatively high resistivities, which shows a peaking point the modelled curve. The fourth geoelectric layer has its resistivities dipping in relation with layer three, with ranges of 103.699 - 537.415 Ωm and thickness of 11.39 m with 20 points well in the range of the driller's log, and thus equally has deviations of ten (10) layers on its resistivities with most VES points' resistivities showing a dropping trend.

The resistivities of geoelectric layer five (5) are declining though still high in eighteen VES points with ranges 104.604 - 492.825 Ωm, an approximated breadth of 15.16 m with thirteen (13) having low resistivities, represents the tuffs. The geoelectric layer six (6) is 12.8 m thick with resistivities between 31.534 - 293.542 Ωm; and geoelectric layer seven (7) is defined by 40.124 - 398.565 Ωm ranges with breadth of 15.49 m, with both representing one lithologic layer of phonolites. The lithologies; red soils (highly weathering formation) as per the driller's log are represented by geoelectric layer eight (8) with breadth of 18.74 m and resistivities' ranges of 28.04 - 99.802 Ωm representing eighteen (18) VES points with thirteen (13) showing deviations to higher resistivities. The geoelectric layer nine (9) has a breadth of 22.68 m and represents two lithologic layers of red soils with particles of tuff and pumice; considering the drillers log, with resistivities' ranges of 25.77 - 99.802 Ωm for twenty (20) VES points, with eleven (11) deviations towards high resistivity. The trachytes represent the lithology well mapped by the ranges of resistivities of 25.77 - 99.802 Ωm which indeed is defined by a

13.07 m thick geoelectric layer ten (10), in which only nine (9) VES points have resistivities deviating upwards.

The geoelectric layer eleven (11) starting from a depth of 139.1 m; marks the water strike level which accordingly is given as 140 m deep from the Olobanita borehole completion records, coinciding with the exact starting depth tuffs. This geoelectric layer has a breadth of 30.18 m and resistivities' ranges of 8.43 - 90.833 Ωm, with only five (5) deviations to marginally high resistivities. There is a correspondence of the resistivities of the eleventh (11) unto the twelve (12) geoelectric layer which is a transition from highly weathered tuffs to highly weathered phonolites as per the driller's log, with both geoelectric layers representing the first aquifer as identified by the borehole completion records. Accordingly, the thirteenth (13) geoelectric layer starting at 186.67 m deep correlates well with the trachytes whose depth starts at 176 m, assuming the driller's log. The resistivities of thirteenth (13), fourteenth (14), and fifteenth (15) geoelectric layers on average are low but distinguishable by their depth ranges of 186.67 - 226.84 m, 226.84 - 249.99 m and 249.99 - 275.45 m defining further three minor aquifers. The three layers are represented by trachytes, tuff and phonolites respectively. The geoelectric layer sixteen (16) is distinct in the depths of 275.45 m - 334.25 m and coincides well with the lithologic layer of brownish formation, as per the driller's log's depth of 274 m - 280 m. This layer is defined with low resistivities which ranges 0.4 - 64 Ωm for 21 VES points and deviations to resistivities above 100 Ωm, for 10 VES points.

4.2. Hydraulic Parameters

The hydraulic parameters (Table 4) covering the hydraulic conductivities and transmissivities for the main aquifer layer (geoelectric layer 13) were calculated using the geoelectric parameters. Notably the geoelectric aquifer layer defined by depth ranges 139.1 - 169.28 m, is also in agreement with the lithologic boundaries representing tuffs outlined by depth 140 - 168 m. Certainly as shown in the Table 2, there is a good correlation between the geoelectric layer thicknesses, the lithologic layer thicknesses and indeed with distinguishable lithologies. From Table 2, the VES point 24 which lies in the proximity of the borehole (Olobanita BH 7), is evident from the correlation and only shows a slight variation where there is representation of two formations (Phonolites and tuffs) by one geoelectric layer, though in some VES points, the two lithologies are discernable.

The results attained in this research (Table 4), the saturated zone, otherwise referred to as the aquifer exhibits a hydraulic conductivity (K) average value of 17.16389314 m/day, in consideration of the ranges 0.248690465 m/day to 74.62681942 m/day, with three outliers whose bulk resistivities are outside the range of the noted aquifer lithology. The VES point near the borehole in consideration has a K of 5.19779643 m/day. There is a direct correlation between the bulk resistivities and the K values, where the increase in resistivity results unto an increase in K values. The values of bulk resistivities and correlated K in

Table 4. Showing aquifer hydraulic parameters.

VES	Starting Depth (m)	Thickness (m)	Bulk resistivity (Ωm)	Formation water resistivity (Ωm)	Formation factor	Hydraulic conductivity (m/day)	Transmissivity (m^2/day)	Longitudinal conductance (Ω^{-1})	Transverse resistance (Ωm^2)	water conductivity μS/cm
VES 1	**139.1**	**47.57**	**8.43**	13.49892	0.624494	0.248690465	11.83021	5.642942	401.0151	740.8
VES 2	**56.32**	**277.93**	**51.85**	13.49892	3.841048	11.07909822	3079.214	5.36027	14410.671	740.8
VES 3	**139.1**	**30.18**	**27.08**	13.49892	2.006086	2.850461648	86.02693	1.114476	817.2744	740.8
VES 4	**139.1**	**30.18**	**45.936**	13.49892	3.402939	8.601607843	259.5965	0.657001	1386.3485	740.8
VES 5	**126.03**	**208.22**	**118.795**	13.49892	8.800334	62.66249182	13047.58	1.752767	24735.495	740.8
VES 6	**139.1**	**30.18**	**35.236**	13.49892	2.610283	4.941758289	149.1423	0.85651	1063.4225	740.8
VES 7	**139.1**	**30.18**	**33.412**	13.49892	2.475161	4.42217241	133.4612	0.903268	1008.3742	740.8
VES 8	**56.32**	**219.13**	**90.833**	13.49892	6.728909	35.76092536	7836.292	2.412449	19904.235	740.8
VES 9	**139.1**	**30.18**	**22.299**	13.49892	1.65191	1.899310471	57.32119	1.353424	672.98382	740.8
VES 10	**139.1**	**30.18**	**587.264**	13.49892	43.50452	1768.240219	53365.49	0.051391	17723.628	740.8
VES 11	**139.1**	**30.18**	**318.207**	13.49892	23.57277	491.2955569	14827.3	0.094844	9603.4873	740.8
VES 12	**139.1**	**136.35**	**21.435**	13.49892	1.587905	1.748749455	238.442	6.361092	2922.6623	740.8
VES 13	**139.1**	**30.18**	**551.002**	13.49892	40.81823	1547.710179	46709.89	0.054773	16629.24	740.8
VES 14	**69.12**	**206.33**	**105.518**	13.49892	7.816773	48.91386652	10092.4	1.955401	21771.529	740.8
VES 15	**139.1**	**47.57**	**33.873**	13.49892	2.509312	4.550652328	216.4745	1.404363	1611.3386	740.8
VES 16	**139.1**	**47.57**	**54.78**	13.49892	4.058102	12.42795125	591.1976	0.868383	2605.8846	740.8
VES 17	**139.1**	**47.57**	**44.309**	13.49892	3.282411	7.977148472	379.473	1.073597	2107.7791	740.8
VES 18	**139.1**	**30.18**	**28.268**	13.49892	2.094093	3.118072617	94.10343	1.067638	853.12824	740.8
VES 19	**139.1**	**47.57**	**61.598**	13.49892	4.56318	15.88084915	755.452	0.772265	2930.2169	740.8
VES 20	**139.1**	**30.18**	**52.677**	13.49892	3.902312	11.45163409	345.6103	0.572926	1589.7919	740.8
VES 21	**103.35**	**123.49**	**39.987**	13.49892	2.962237	6.437093865	794.9167	3.088254	4937.9946	740.8
VES 22	**126.03**	**60.64**	**129.154**	13.49892	9.567728	74.62681942	4525.37	0.469517	7831.8986	740.8
VES 23	**139.1**	**47.57**	**82.491**	13.49892	6.110933	29.23945211	1390.921	0.576669	3924.0969	740.8
VES 24	**139.1**	**47.57**	**36.098**	13.49892	2.67414	5.19779643	247.2592	1.317802	1717.1819	740.8
VES 25	**126.03**	**43.25**	**87.993**	13.49892	6.518521	33.46386373	1447.312	0.491516	3805.6973	740.8
VES 26	**56.32**	**112.96**	**61.483**	13.49892	4.554661	15.81894652	1786.908	1.837256	6945.1197	740.8
VES 27	**84.61**	**190.84**	**57.819**	13.49892	4.283232	13.9125586	2655.073	3.300645	11034.178	740.8
VES 28	**139.1**	**30.18**	**68.804**	13.49892	5.097	20.0120744	603.9644	0.438637	2076.5047	740.8
VES 29	**139.1**	**47.57**	**77.808**	13.49892	5.764017	25.87737323	1230.987	0.611377	3701.3266	740.8
VES 30	**84.61**	**84.67**	**36.329**	13.49892	2.691252	5.267556464	446.004	2.330645	3075.9764	740.8
VES 31	**139.1**	**136.35**	**54.297**	13.49892	4.022322	12.20003277	1663.474	2.511188	7403.396	740.8

ascending order is given as; 8.4 Ωm, 0.248690465 m/day; 21.435 Ωm, 1.748749455 m/day; 22.299 Ωm, 1.899310471 m/day; 27.08 Ωm, 2.850461648 m/day; 28.27 Ωm, 3.118072617 m/day; 33.412 Ωm, 4.42217241 m/day; 33.87 Ωm, 4.550652328 m/day; 35.236 Ωm, 4.941758289 m/day; 36.098 Ωm, 5.19779643 m/day; 36.329 Ωm, 5.267556464 m/day; 39.987 Ωm, 6.437093865 m/day; 44.309 Ωm, 7.977148472 m/day; 45.936 Ωm, 8.601607843 m/day; 51.85 Ωm, 11.07909822 m/day; 52.677 Ωm, 11.45163409 m/day; 54.297 Ωm, 12.20003277 m/day; 54.78 Ωm, 12.42795125 m/day; 57.819 Ωm, 13.9125586 m/day; 61.483 Ωm, 15.81894652 m/day; 61.6 Ωm, 15.88084915 m/day; 68.804 Ωm, 20.0120744 m/day; 77.808 Ωm, 25.87737323 m/day; 82.491 Ωm, 29.23945211 m/day; 87.993 Ωm, 33.46386373 m/day; 90.833 Ωm, 35.76092536 m/day; 105.518 Ωm, 48.91386652 m/day; 118.8 Ωm, 62.66249182 m/day; 129.15 Ωm, 74.62681942 m/day; 318.21 Ωm, 491.2955569 m/day; 551 Ωm, 1547.710179 m/day; 587.26 Ωm, 1768.240219 m/day.

The aquifer transmissivities shown in Table 4 are given as the hydraulic conductivities multiplied by the aquifer thickness as defined by geoelectric layer thickness in the case of relying on the VES surveys. In the present study the aquifer is defined by geoelectric layer ranges given as 30.18 m thickness covering 35.48 percent, thicknesses 47.57 m (25.8 percent), 136.35 m (6.4 percent), 43.25 m, 60.64 m and 84.67 m, 112.96 m, 123.49 m, 190.84 m, 206.33 m, 208.22 m, 219.13 m, 277.93 m thicknesses representing 3.33 percent each. For equal thicknesses of 30.18 m, the T values varied from a minimum of 57.32119 Ωm^2 at VES 9 to 53365.49 Ωm^2 at VES 10; for 47.57 m has a range between 11.83021 Ωm^2 for VES 1 and 1390.921 Ωm^2.

Similarly, the Dar'Zarrouk's parameters (longitudinal conductance and transverse resistance) were computed (Table 4). The aquifer thickness have a bearing on the values of longitudinal unit conductance by taking the two aspects, the precise geoelectric thickness (~47.57 m) determined to be matching the lithologic thickness (36 m). The longitudinal unit conductance is inversely proportional to the geoelectric layer resistivities and directly proportional to layer thickness. The variance of longitudinal unit conductance shows that 63.15 percent of the aquifer area matching well with lithologic formations is having lowest values of S (<1.0 Ω^{-1}), an indication that the resistivity values of these points are relatively high when compared to their corresponding thickness. Notably, where the geoelectric layer surpass and is rather represented by more than one lithologic layer, the longitudinal unit conductance about 83.33 percent have high values f S (~1.1 - 5.3 Ω−1). There is no large disparities of the resistivities between the geoelectric layers, thus when there is an increase in geoelectric layer thickness there is correlated increase in the longitudinal unit conductance.

The transverse resistance values shown in Table 4 have a direct proportionality to both the aquifer layer thickness and the geoelectric layer resistivities. The aquifer layer geoelectric thicknesses can be mapped unto several batches; 30.18 m thickness covering 35.48 percent, thicknesses 47.57 m (25.8 percent), 136.35 m (6.4 percent), 43.25 m, 60.64 m and 84.67 m, 112.96 m, 123.49 m, 190.84 m,

206.33 m, 208.22 m, 219.13 m, 277.93 m thicknesses representing 3.33 percent each. Evidently, using the close range of resistivities recorded indicates that indeed that transverse resistance increases with increase in aquifer thickness. For example, for resistivities 52.677 Ω, 54.78 Ω, 54.297 Ω, 57.819 Ω, and 51.85 Ω, for 30.18 m, 47.57 m, 136.35 m, 190.84 m, 277.93 m thicknesses respectively, have their correlated transverse resistances values notably rising incrementally, from 1589.7919 Ωm^2, 2605.8846 Ωm^2, 7403.396 Ωm^2, and 11034.178 Ωm^2 correspondingly.

5. Discussion

The results obtained in the study area present varying layer characteristics. The range of resistivity values (Table 3) and a constrained correspondence to different lithological units has been done using VES 24 done near the drilled site Olbanita BH 7, whose geological parameters correlated with the borehole's log lithology as shown in Table 2, and Figure 3. The analysis of the geoelectric layer thickness and resistivities shown in Table 3, displays a good agreement between the VES points. With the basis of the correlation signatures, inference of lithology was achieved at other VES points for the delineation of surface lithology.

The first geoelectric unit which has a corresponding breadth (b) of 8.62 m, represents the surface volcanic soils (Figure 3) showing a resistivity range of 55.01 Ωm to 158.474 Ωm (Table 3) with an average of 99.87 Ωm. Exceptionally, VES points 4 and 6 present b of 18.86 m, though with resistivities being within range of the others. The variations of the top layer's resistivity values are attributed to presence of gravels and coarse sands and prevailing conditions at the measured VES points. Demarcation of geoelectric layer 2 marking tuffs, agree in the order of 93.55 percent of VES points, having b of 10.24 m and resistivity ranges of 24.265 Ωm to 147.7 Ωm, with an average of 54.73 Ωm. Geoelectric layers 3 and 4 are represented by pyroclastics, though distinctly mapped as breadths 10.91 m (90.32 percent of VES points) and 11.39 m (64.51 percent of VES points). The resistivity ranges are considered to be relatively high, at greater than 100 Ωm (129.851 Ωm to 1047.042 Ωm) in layer 3 compared to an average of 335.82 Ωm with 74.19 percent of VES points being within the range and at 67.74 percent of VES points for layer 4 at greater than 100 Ωm (103.699 Ωm to 537.415 Ωm) compared to an average of 185.13 Ωm. The posting of two different geoelectric layers within the same lithologic formation, shows a phase of material compaction that brings about the differences in vertical resistivities. The geoelectric layers 5, 6, 7, 8, and 9 have resistivity averages of 164.87 Ωm, 134.88 Ωm, 127.74 Ωm, 120.61 Ωm, 114.99 Ωm respectively. The lithologies in question are tuffs, phonolites, red formation (highly weathered soils) with particles of tuff and pumice, of which their relatively high resistivity values are attributed to manifestation of larger quantities of gravels and coarse sands.

The aquifer regimes are well mapped and well portrayed in geoelectric layers 10, 11 and 12, 13, 14 and 15, which portent resistivity value averages of 97.69 Ωm, 92.60 Ωm, 93.21 Ωm, 82.31 Ωm and 81.33 Ωm, respectively. The 10th geoe-

lectric layer, represents the probable capillary fringe or the sub saturated zone whose depth ranging from 126.03 - 139.1 m, and the layer exhibits resistivities' range of 25.77 - 344.88 Ωm, with 70.96 percent being below 100 Ωm. The lithologic formation is qualified as trachytes occurring between 122 - 140 m deep according to the driller's log. There are four distinct aquifers in the study area and are identified both by change of lithologies and confirmed by water strike levels of 140 m, 182 m, 208 m, and 238 m depths in the area. The first aquifer is defined by a depth range of 139.1 m to 186.67 m, which coincides well with the water strike level of the first aquifer of 140 m deep. This system is defined by lithologies of weathered tuffs covering a breadth of 30.18 m underlain by weathered phonolites with a breadth of 17.39 m. This forms the main aquifer under consideration in the study. The second aquifer is defined by fissured trachytes with a breadth of 29.09 m occurring in the depth range of 186.67 - 226.84 m. The third aquifer geoeletrically is in the depth ranges of 226.84 - 249.99 m and defined by tuffs underlying the phonolites. The fourth and final aquifer is represented by the phonolites in the depths of 249.99 - 275.45 m. the 16th geoelectric layer has increased resistivity values at an average of 176.94 Ωm, indicating an end to the aquifer regime.

The results given by the geoelectric layer resistivities in the main aquifer that is defined by depths 139.1 - 186.67 m and their associated breadths show that 64.61 percent is represented by 30.18 m to 47.57 m thickness ranges. The average hydraulic conductivities are 11.30358053 m/day and transmissivities are 258.0687812 m^2/day with the exclusion of outliers noted in VES 10, VES 11, VES 13 and VES 22, which indicates relatively high bulk resistivities in consideration of the VES points whose geoelectric thickness fall in the approximated aquifer thickness. The ranges of K are 0.248690465 Ω to 48.91386652 Ω and T of 11.8302054 Ωm^2 to 1447.312106 Ωm^2, with K being directly proportional to T. The geology of the study area is defined as volcano sedimentary in nature, and thus a correlation between the ranges of the K and T as determined by this study fall within the documented range values. These ranges of calculated K values are well within 2.487×10^{-1} m/day to 1.768×10^{3} m/day, which in the volcano sedimentary ranges falls between the values 10^{-2} m/day for silt, semiconsolidated sandstone, fractured basalt, (or otherwise equivalent volcanic rocks), to 10^{3} m/day for gravel and also fractured volcanic rocks as per the hydraulic conductivities of selected consolidated and unconsolidated geologic materials presented by Heath (1983).

The main aquifer lithologies are tuffs (yellow), tuffs (reddish brown), tuffs (greyish), tuffs (weathered) vertically stratified top to bottom in that order. There is a relative observation that aquifer transmissivities can be estimated more accurately if the values are sorted by standard geoelectric layers thus considered as hydraulic units. The Hydraulic conductivities are also noted t be dissimilar in different directions at any place in an aquifer. Fr example in the horizontal perspective, considering the same lithology in breadth covering the aquifer in the study area, there are different hydraulic conductivities. For instance in the geoelectric layer having breadth of 30.18 m, in VES points 3, 4, 6, 7, 9, 10, 11, 13, 18,

20, 28 have K values of 2.850461648 m/day, 8.601607843 m/day, 4.941758289 m/day, 4.42217241 m/day, 1.899310471 m/day, 1768.240219 m/day, 491.2955569 m/day, 1547.710179 m/day, 3.118072617 m/day, 11.45163409 m/day, 20.0120744 m/day. This case indicates that hydraulic conductivity is different from place to place in the same aquifer having a rock made up of tuffs, thus accordingly defining the aquifer to be heterogeneous (Heath, 1983), that is, an aquifer whose hydraulic conductivity differs from one part of the area to another. There isn't noticeable variation in vertical hydraulic conductivities within the marked aquifer covering the thickness of 30.18 m made up of the tuffs.

Transmissivity is defined as the capacity of an aquifer to transmit water of the dominant kinematic viscosity and it is equated to the hydraulic conductivity of the aquifer multiplied by the saturated breadth of the aquifer. It is clear then that unless the K is the same across, and equally b remains the same, then T value will differ in different places in the same aquifer given its dependence on both K and b. This fact is clearly enumerated in a part of the considered aquifer in this study which has the same b, but gives different T values. Despite the VES points 3, 4, 6, 7, 9, 10, 11, 13, 18, 20, 28 having same b value of 30.18 m, they present differing T values of 86.02693 m^2/day, 259.5965 m^2/day, 149.1423 m^2/day, 133.4612 m^2/day, 57.32119 m^2/day, 53365.49 m^2/day, 14827.3 m^2/day, 46709.89 m^2/day, 94.10343 m^2/day, 345.6103 m^2/day, 603.9644 m^2/day. The differences in either K or T values in the same lithologic formation are caused by slight differences in mineralogy, different levels of weathering, and to some extent the cementing material.

6. Conclusion

The VES method has been successfully used in defining the aquifer regimes as noted in the analysis that well compares with the drillers log data. There are four distinct aquifers in the study area and are identified by geoelectric layer depth ranges 139.1 - 186.67 m, 186.67 - 226.84 m, 226.84 - 249.99 m, and 249.99 - 275.45 m, with a good correlation with change depth ranges of lithologies at 140 - 176 m (140 - 168 m for weathered tuffs and 168 - 176 m for weathered phonolites), 176 - 230 m defined by fissured trachytes, 230 - 252 m (230 - 242 m with Tuffs and 242 - 252 m with Phonolites) and 252 - 274 m (252 - 270 m with Phonolites and 270 - 274 m with Trachytes). Notably, there is a good covenant by water strike levels marking the starting depths of the different aquifers at 140 m, 182 m, 208 m, and 238 m depths in the area.

The main aquifer is considered to be heterogeneous given the noted horizontal changes in both hydraulic conductivities and transmissivities across the 31 VES points done in the study area.

Acknowledgements

Special thanks go to Water Resources Authority, Kenya, and the Rift Valley Water services Board for provision of requested data. Equally, we acknowledge the support of Ministry of Petroleum and Mining, Kenya from whom geological

maps were obtained, which were useful in production the final geological map of the area. Finally, my gratitude to Fred who was instrumental in fieldworks.

Conflicts of Interest

The author declares no conflicts of interest regarding the publication of this paper.

References

Archie, G. (1942). The Electrical Resistivity Log as an Aid in Determining Some Reservoir Characteristics. *Petroleum Transactions of the American Institute of Mineralogical and Engineers, 146,* 54-62. https://doi.org/10.2118/942054-G

Archie, G. (1950). Introduction to Petrophysics of Reservoir Rocks. *American Association of Petroleum Geologists Bulletin, 34,* 943-961.

Byun, Y.-H., Hong, W.-T., & Yoon, H.-K. (2019). Characterization of Cementation Factor of Unconsolidated Granular Materials through Time Domain Reflectometry with Variable Saturated Conditions. *Materials, 12,* Article 1340. http://www.mdpi.com/journal/materials https://doi.org/10.3390/ma12081340

Carmen, D.C. (1956). *Flow of Gases through Porous Media* (182 p). Academic Press.

Carothers, J. E. (1968). A Statistical Study of the Formation Relation. *The Log Analyst, 9,* 13-20.

Carothers, J. E., & Porter, C. R. (1970). Formation Factorporosity Relation Derived from Well Log Data. *11th Annual Logging Symposium*, Los Angeles, 3-6 May 1970, A1-A19.

Hamada, G. M., Almajed, A. A., Okasha, T. M., & Algathe, A. A. (2012). Uncertainty Analysis of Archie's Parameters Determination Techniques in Carbonate Reservoirs. *Journal of Petroleum Exploration and Production Technology, 3,* 1-10. https://doi.org/10.1007/s13202-012-0042-x

Heath, R. C. (1983). *Basic Ground-Water Hydrology: U.S.* (86 p). Geological Survey Water-Supply Paper 2220.

Kozeny, J. (1953). *Hydraulics* (pp. 546-549). Springer.

McCall, G. J. R. (1967). *Geology of Nakuru-Thompson Falls—Lake Rannington Area*. Geological Survey of Kenya, Rep 78, 122 p. Publ. No. 4271.

Nutting, P. G. (1930). Physical Analysis of Oil Sands. *American Association of Petroleum Geologist Bulletin, 14,* 1337-1349. https://doi.org/10.1306/3D932938-16B1-11D7-8645000102C1865D

Nyaberi, D. M. (2010). *Geophysical Characterization of the Lithology and Structure of the Olobanita Well Field, Lower Lake Baringo Basin, Kenya Rift: Implication on Groundwater Occurrence* (p. 118). Masters' Dissertation, University of Nairobi.

Nyaberi, D. M. (2020). *Delineation of Groundwater Potential Zones in Arid and Semi-Arid Lands Using Integrated Approaches of Remote Sensing, Geophysical Techniques and Borehole Data: A Case Study from Turkana South Sub-County, Kenya* (p. 303). PhD Thesis, Kisii University.

Olago, D. O. (2018). Constraints and Solutions for Groundwater Development, Supply and Governance in Urban Areas in Kenya. *Hydrogeology Journal, 27,* 1031-1050. https://doi.org/10.1007/s10040-018-1895-y

Pinas, A., & Elias, R. M. (2019). *Impact of Tortuosity and Cementation Factor in Water Saturation Calculations in Heterogeneous Sands of the Tambaredjo Field, Guiana Ba-*

sin, Suriname. https://www.researchgate.net/publication/333356245

Rhett, H. (2001). An Introduction to Electrical Resistivity in Geophysics. *American Journal of Physics, 69,* 943-952. https://doi.org/10.1119/1.1378013

Salem, H. S. (2001). Modeling of Lithologic and Hydraulic Conductivity of Shallow Sediments from Resistivity Measurements Using Schlumberger Vertical Electrical Soundings. *Energy Sources, 23,* 599-618. https://doi.org/10.1080/00908310119202

Sethi, D. K. (1979). Some Considerations about the Formation Resistivity Factor-Porosity Relations. *SPWLA 20th Annual Logging Symposium*, Tulsa, 3-6 June 1979.

Sirles, P. C. (2006). *NCHRP Synthesis 357: Use of Geophysics for Transportation Projects*. Transportation Research Board for National Academies. http://onlinepups.trb.org/onlinepups/nchrp/nchrp_syn_357.pdf

Sosi, B. (2020). *Hydraulic Characteristics of Olbanita Aquifer System in Lower Baringo Basin of the Rift Valley of Kenya: Implications on Groundwater Yields* (303 p). PhD Thesis, Kisii University.

Sosi, B., Getabu, A., & Maobe, S. (2019). Groundwater Evolutionary Processes and Quality Characterization: A Case of Olbanita Aquifer System, Lower Baringo Basin, Kenya Rift. *Journal of Soil and Water Sciences, 3,* 91-101. https://doi.org/10.36959/624/434

Winsauer, W. O., Shearin Jr., H. M., Masson, P. H., & Williams, M. (1952). Resistivity of Brine-Saturated Sands in Relation to Pore Geometry. *American Association of Petroleum Geologists Bulletin, 36,* 253-277. https://doi.org/10.1306/3D9343F4-16B1-11D7-8645000102C1865D

Appendix

Table A1. VES correlation of the layer models obtained from the apparent resistivity representing the 31 VES points.

Geoelectric Layer	1			2			3			4			5			6			7			8			9			10			11			12			13			14			15			16			
	Starting Depth (m)	Breadth (m)	Resistivity (Ωm)	Starting Depth (m)	Breadth (m)	Resistivity (Ωm)	Starting Depth (m)	Breadth (m)	Resistivity (Ωm)	Starting Depth (m)	Breadth (m)	Resistivity (Ωm)	Starting Depth (m)	Breadth (m)	Resistivity (Ωm)	Starting Depth (m)	Breadth (m)	Resistivity (Ωm)	Starting Depth (m)	Breadth (m)	Resistivity (Ωm)	Starting Depth (m)	Breadth (m)	Resistivity (Ωm)	Starting Depth (m)	Breadth (m)	Resistivity (Ωm)	Starting Depth (m)	Breadth (m)	Resistivity (Ωm)	Starting Depth (m)	Breadth (m)	Resistivity (Ωm)	Starting Depth (m)	Breadth (m)	Resistivity (Ωm)	Starting Depth (m)	Breadth (m)	Resistivity (Ωm)	Starting Depth (m)	Breadth (m)	Resistivity (Ωm)	Starting Depth (m)	Breadth (m)	Resistivity (Ωm)	Starting Depth (m)	Breadth (m)	Resistivity (Ωm)	Starting Depth (m)
VES 1	0	8.62	74.08	8.62	10.24	26.07	18.86	22.3 m breadth 635.86 Ωm					41.16	15.16	397.52	56.32	12.8	234.13	69.12	15.49	140.27	84.61	18.74	72.81	103.35	35.75 m breadth 25.77 Ωm					139.1	47.57 m breadth 8.43 Ωm					186.67	40.17	4.14	226.84	23.15	6.07	249.99	25.46	4.26	275.45	58.8	0.4	334.25
VES 2	0	8.62	55.01	8.62	10.24	147.7	18.86	10.91	245.94	29.77	26.55 m breadth 26.96 Ωm					56.32	277.93 m breadth 51.85 Ωm																																	334.25
VES 3	0	8.62	72.33	8.62	10.24	45.64	18.86	10.91	542.34	29.77	11.39	212.76	41.16	15.16	111.5	56.32	12.8	75.8	69.12	15.49	52.97	84.61	41.42 m breath 28.04 Ωm					126.03	13.07	42.27	139.1	30.18	27.08	169.28	164.97 m breadth 64 Ωm														334.255
VES 4	0	18.86 m breadth 67.369 Ωm					18.86	10.91	733.543	29.77	11.39	200.681	41.16	15.16	73.57	56.32	69.71 m breadth 45.534 Ωm											126.03	13.07	60.696	139.1	30.18	45.936	169.28	106.17 m breadth 69.15 Ωm											275.45	58.8	154.236	334.25
VES 5	0	8.62	70.488	8.62	10.24	126.576	18.86	10.91	750.418	29.77	11.39	136.847	41.16	43.45 m breadth 47.496 Ωm								84.61	41.42 m breadth 89.06 Ωm					126.03	208.22 m breadth 118.795 Ωm																				334.25
VES 6	0	18.86 m breadth 58.813 Ωm					18.86	10.91	651.997	29.77	11.39	177.517	41.16	15.16	122.875	56.32	12.8	96.534	69.12	15.49	65.08	84.61	41.42 m breadth 32.463 Ωm					126.03	13.07	48.165	139.1	30.18	35.236	169.28	106.17 m breadth 62.561 Ωm											275.45	58.8	138.45	334.25
VES 7	0	8.62	61.39	8.62	10.24	102.738	18.86	10.91	61.164	29.77	11.39	537.415	41.16	15.16	313.473	56.32	12.8	109.938	69.12	15.49	53.306	84.61	54.49 m breadth 32.243 Ωm								139.1	30.18	33.412	169.28	17.39	47.237	186.67	88.78 m breadth 33.956 Ωm								275.45	58.8	10.616	334.25
VES 8	0	8.62	86.266	8.62	10.24	38.326	18.86	22.3 m breadth 207.978 Ωm					41.16	15.16	157.701	56.32	219.13 m breadth 90.833 Ωm																													275.45	58.8	37.759	334.25
VES 9	0	8.62	128.154	8.62	10.24	69.28	18.86	10.91	30.226	29.77	11.39	462.162	41.16	15.16	492.825	56.32	12.8	273.701	69.12	15.49	139.017	84.61	18.74	64.26	103.35	35.75 m breadth 31.974 Ωm					139.1	30.18	22.299	169.28	17.39	43.986	186.67	40.17	29.09	226.84	48.61 m breadth 50.575 Ωm					275.45	58.8	41.293	334.25
VES 10	0	8.62	131.754	8.62	21.15 m breadth 56.234 Ωm					29.77	26.55 m breadth 54.415 Ωm					56.32	12.8	82.677	69.12	15.49	152.642	84.61	18.74	311.47	103.35	22.68	527.35	126.03	13.07	337.247	139.1	30.18	587.264	169.28	17.39	330.291	186.67	40.17	400.583	226.84	107.41 m breadth 198.838 Ωm								334.25
VES 11	0	8.62	138.215	8.62	10.24	47.051	18.86	10.91	132.723	29.77	11.39	19.559	41.16	15.16	50.593	56.32	12.8	197.785	69.12	15.49	398.565	84.61	41.42 m breadth 601.786 Ωm					126.03	13.07	315.037	139.1	30.18	318.207	169.28	164.97 m breadth 126.925 Ωm														334.25
VES 12	0	8.62	78.885	8.62	10.24	33.011	18.86	10.91	150.283	29.77	11.39	21.72	41.16	15.16	58.118	56.32	47.03 m breadth 90.04 Ωm								103.35	35.75 m breadth 40.658 Ωm					139.1	136.35 m breadth 21.435 Ωm														275.45	58.8	15.165	334.25
VES 13	0	8.62	158.474	8.62	10.24	21.06	18.86	10.91	143.536	29.77	26.55 m breadth 15.482 Ωm					56.32	12.8	31.534	69.12	15.49	63.872	84.61	18.74	138.912	103.35	35.75 m breadth 344.885 Ωm					139.1	30.18	551.002	169.28	17.39	386.874	186.67	40.17	645.675	226.84	48.61 m breadth 315.04 Ωm					275.45	58.8	1059.309	334.25
VES 14	0	8.62	113.219	8.62	10.24	19.953	18.86	10.91	184.676	29.77	26.55 m breadth 375.371 Ωm					56.32	12.8	156.589	69.12	206.33 m breadth 105.518 Ωm																										275.45	58.8	532.267	334.25
VES 15	0	8.62	85.422	8.62	10.24	41.361	18.86	10.91	143.494	29.77	11.39	48.246	41.16	15.16	215.865	56.32	28.29 m breadth 293.542 Ωm					84.61	18.74	187.864	103.35	22.68	103.411	126.03	13.07	66.62	139.1	47.57 m breadth 33.873 Ωm					186.67	88.78 m breadth 19.419 Ωm								275.45	58.8	8.792	334.25
VES 16	0	8.62	85.115	8.62	10.24	53.557	18.86	10.91	70.701	29.77	11.39	84.895	41.16	43.45 m breadth 253.735 Ωm								84.61	18.74	202.053	103.35	22.68	138.056	126.03	13.07	95.932	139.1	47.57 m breadth 54.78 Ωm					186.67	88.78 m breadth 24.806 Ωm								275.45	58.8	5.34	334.25
VES 17	0	8.62	77.659	8.62	10.24	36.625	18.86	10.91	236.325	29.77	11.39	83.955	41.16	43.45 m breadth 236.715 Ωm								84.61	18.74	167.655	103.35	22.68	100.785	126.03	13.07	71.828	139.1	47.57 m breadth 44.309 Ωm					186.67	40.17	31.07	226.84	48.61 m breadth 41.199 Ωm					275.45	58.8	19.167	334.25
VES 18	0	8.62	82.021	8.62	10.24	56.208	18.86	10.91	129.851	29.77	26.55 m breadth 374.697 Ωm					56.32	12.8	207.108	69.12	15.49	107.313	84.61	18.74	51.602	103.35	35.75 m breadth 32.539 Ωm					139.1	30.18	28.268	169.28	57.56 m breadth 47.593 Ωm					226.84	107.41 m breadth 127.829 Ωm								334.25

Continued

VES 19	0	8.62	71.848	8.62	10.24	44.602	18.86	10.91	377.12	29.77	73.58 m breadth 140.604 Ωm														103.35	35.75 m breadth 104.476 Ωm					139.1	47.57 m breadth 61.598 Ωm					186.67	88.78 m breadth 36.845 Ωm								275.45	58.8	12.364	334.25
VES 20	0	8.62	143.34	8.62	10.24	36.801	18.86	10.91	405.844	29.77	26.55 m breadth 112.332 Ωm					56.32	47.03 m breadth 251.418 Ωm								103.35	22.68	162.151	126.03	13.07	102.525	139.1	30.18	52.677	169.28	17.39	31.761	186.67	88.78 m breadth 11.105 Ωm								275.45	58.8	1.668	334.25
VES 21	0	8.62	130.131	8.62	10.24	80.378	18.86	10.91	28.512	29.77	11.39	347.561	41.16	15.16	354.906	56.32	12.8	184.09	69.12	15.49	94.982	84.61	18.74	50.04	103.35	123.49 m breadth 39.987 Ωm														226.84	48.61 m breadth 84.15 Ωm					275.45	58.8	207.147	334.25
VES 22	0	8.62	111.113	8.62	10.24	41.812	18.86	10.91	138.979	29.77	26.55 m breadth 79.599 Ωm					56.32	12.8	138.256	69.12	56.91 m breadth 196.776 Ωm								126.03	60.64 m breadth 129.154 Ωm								186.67	88.78 m breadth 64.143 Ωm								275.45	58.8	18.699	334.25
VES 23	0	8.62	132.11	8.62	10.24	76.023	18.86	10.91	40.285	29.77	39.35 m breadth 111.12 Ωm								69.12	34.23 m breadth 167.129 Ωm					103.35	35.75 m breadth 138.915 Ωm					139.1	47.57 m breadth 82.491 Ωm					186.67	88.78 m breadth 44.74 Ωm								275.45	58.8	15.945	334.25
VES 24	0	8.62	156.089	8.62	10.24	93.402	18.86	10.91	35.952	29.77	11.39	82.123	41.16	43.45 m breadth 248.41 Ωm								84.61	18.74	163.673	103.35	22.68	94.541	126.03	13.07	63.189	139.1	47.57 m breadth 36.098 Ωm					186.67	40.17	24.561	226.84	48.61 m breadth 33.721 Ωm					275.45	58.8	16.572	334.25
VES 25	0	8.62	152.18	8.62	10.24	24.265	18.86	10.91	646.992	29.77	11.39	148.114	41.16	15.16	53.917	56.32	69.71 m breadth 40.124 Ωm											126.03	43.25 m breadth 87.993 Ωm					169.28	17.39	159.035	186.67	88.78 m breadth 317.3 Ωm								275.45	58.8	1815.026	334.25
VES 26	0	8.62	144.374	8.62	10.24	24.888	18.86	10.91	576.439	29.77	11.39	133.599	41.16	15.16	82.646	56.32	112.96 m breadth 61.483 Ωm																	169.28	106.17 m breadth 126.096 Ωm											275.45	58.8	328.977	334.25
VES 27	0	8.62	106.328	8.62	10.24	27.942	18.86	10.91	639.865	29.77	11.39	163.859	41.16	15.16	104.604	56.32	28.29 m breadth 83.079 Ωm					84.61	190.84 m breadth 57.819 Ωm																							275.45	58.8	50.083	334.25
VES 28	0	8.62	104.319	8.62	10.24	28.635	18.86	10.91	1047.042	29.77	11.39	244.941	41.16	15.16	62.922	56.32	69.71 m breadth 43.404 Ωm											126.03	13.07	91.403	139.1	30.18	68.804	169.28	17.39	99.673	186.67	63.32 m breadth 69.105 Ωm					249.99	84.26 m breadth 40.526 Ωm					334.25
VES 29	0	8.62	79.379	8.62	10.24	53.203	18.86	10.91	536.874	29.77	11.39	103.699	41.16	97.94 m breadth 99.802 Ωm																	139.1	47.57 m breadth 77.808 Ωm					186.67	88.78 m breadth 44.119 Ωm								275.45	58.8	12.267	334.25
VES 30	0	8.62	57.599	8.62	10.24	77.028	18.86	10.91	165.986	29.77	11.39	243.331	41.16	15.16	214.966	56.32	12.8	137.794	69.12	15.49	77.982	84.61	84.67 m breadth 36.329 Ωm											169.28	57.56 m breadth 51.992 Ωm					226.84	48.61 m breadth 79.353 Ωm					275.45	58.8	218.987	334.25
VES 31	0	8.62	82.695	8.62	10.24	40.097	18.86	10.91	663.094	29.77	11.39	151.614	41.16	97.94 m breadth 66.341 Ωm																	139.1	136.35 m breadth 54.297 Ωm														275.45	58.8	35.961	334.25